Characterization of two sludges from a pyrometallurgical copper smelting complex for designing a Se and Pb recovery proposal

D.C. Paz-Gómez[1], S.M. Pérez-Moreno[1], I. Ruiz-Oria[2], G. Ríos[2] and J.P. Bolívar[1]

[1]Department of Integrated Sciences, University of Huelva, Huelva, Spain

[2]Atlantic Copper S.L.U, Huelva, Spain

E-mail address: daniela.paz@dci.uhu.es

Telephone number: +34959219798

Abstract

Gas scrubbing sludge (SS) and fine dust of converters (SC) are wastes generated in the off-gas cleaning system of smelting and converting processes. Both wastes are considered hazardous materials due to their high metal contents and leaching characteristics. The main purpose of this study was to gain essential knowledge on the recovery of valuable elements contained in these wastes. Thus, an exhaustive characterization was carried out to determine the composition, mineral phases, particle size, and leachability of both wastes (SS and SC) as a preliminary step to select the most appropriate applications and treatment for them. These wastes are composed of fine particles (~ 95 % < 63 μm), mainly containing Pb (> 20 %) as anglesite ($PbSO_4$), while SS presents a high concentration of Se (34 %), which is mainly identified as metallic selenium. Therefore, these residues could be used as secondary sources of Pb and Se. The recovery of Se by roasting process and Pb recovery by hydrometallurgical route seem to be the best options for the management of these wastes.

Keywords: Converter dust, Gas scrubbing sludge, Selenium recovery, Copper smelting, sludge characterization.

Graphical abstract

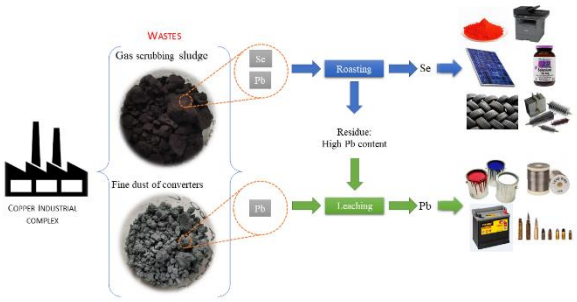

Statement of Novelty

This study is new to Waste & Biomass Valorization, because it is the first time that these two wastes from copper smelting are deeply characterized and proposed a viable pathway for their valorization.

1. Introduction

The global demand for copper has increased in the last 50 years due to expanding sectors such as electrical and electronic components, building construction, manufacture of industrial machinery and equipment, transport and consumer products. Refined copper production worldwide reached 23.5 million tonnes in 2017 [1], which accompanies a huge amount of dust, sludge, slag and wastewater [2, 3]. In the last decades, the recycling and valorisation increase of the industrial wastes has reduced disposal costs and prevented risks for the environment and human health [4, 5].

A big hydro-pyrometallurgical copper industrial complex is located in Huelva (Spain), which is one of the biggest manufacturers of copper cathodes in Europe, which produces around $2.9 \cdot 10^5$ t/y of high purity copper (99.99 % Cu). The industrial process (Fig. 1) begins with the smelting of copper concentrate (around 30 % Cu), in the Flash Furnace (FF), in which the "matte" with 64 % Cu is obtained. Then, the matte is introduced into the Converter Furnaces (CF), where it becomes "blister copper" (> 99 % Cu). The slag generated in the FF and CF is treated in an Electric Furnace (EF) to recover the remaining copper in the slags (1.5 % and 5 %, respectively), leaving the final copper content below 1 % in the obtained slag from the EF, which is mainly formed by iron silicates (Fig. 1). The blister copper is transformed into "copper anodes" (99.6 % Cu, $3.3 \cdot 10^5$ t/y) in the Refining Furnaces (RF). Finally, the anodes are subjected to the electro-refining step, in which "copper cathodes" are obtained (> 99.99 % Cu).

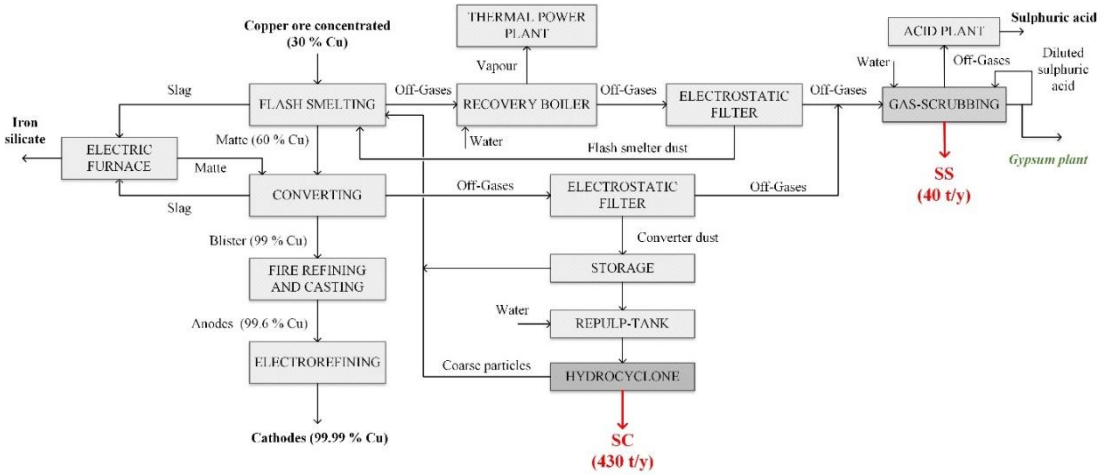

Fig. 1. Overview of material flows and process.

Smelting copper concentrate in the FF is a continuous process in which O_2-erinched air is blown and dried concentrate, flux agent (SiO_2) and recycled materials come from different steps of the process at 1250 ºC.

The copper concentrate (raw material with about 30% in Cu) reacts with O_2 to form molten iron-silicate (slag) and Cu-enriched molten sulphide phase (matte, in which the copper content is still rather low, about 60%), is a solution composed mainly by Cu_2S and FeS. And then the slag and matte are separated due to their different densities. In addition, most of the sulphur contained in the raw material goes out as SO_2-rich off-gas [6, 7].

The SO_2-rich gases from FF are cooled in a heat recovery boiler (Fig. 1), where a high-pressure steam is produced, which generates electricity. Then, the outgoing gases from the boiler are dedusted in electrostatic filters, and the collected dusts are returned to FF. On the other hand, the dedusted gases coming from both FF and CF electrofilters are mixed and introduced into the scrubber section, where the smallest particles and some soluble gases are removed by using diluted acid. And finally, the precipitated solids (Sludge Scrubber = SS) are collected in a decanter. About 40 t/y of SS are produced and stored in a controlled landfill located 70 km from Huelva city [6, 8].

On the other hand, the matte is oxidized using O_2-enriched air, in the CF. This conversion is a batch process in two stages: the slag and copper blows. The first stage is the slag blow, in which FeS is oxidized to produce slag. This stage is ended when there is about 1% Fe in the matte; then, the slag is removed, producing a matte with a low S content (white metal), which is oxidized to blister copper. The converting process is finished when oxide copper begins to appear in the copper sample. Both stages generate SO_2-enriched off-gases [6].

Off-gases from CF are dusted off in electrostatic filters (see figure 1), and purified gases, previously mixed with off-gases from FF, are sent to the scrubber section. About 70 % of the converter dust collected in these filters is sent to FF, whereas the remaining 30 % of this dust (around 1100 t/y) is sent to hydro-cyclones, where the coarse particles are separated from fine particles (< 15 μm). Previous studies indicated that the valuable metals (copper and gold) are found in the coarse particles, which are recycled into FF, whereas the impurities (As, Bi, Sb, Pb and Zn), are contained in the fine particles, forming a final sludge composed of fine dust of converters (SC), which are disposed by landfill at around 430 t/y [8]. Both wastes are currently disposed in a controlled landfill for hazardous wastes, where they are managed by applying a stabilization process to reduce the mobility of pollutants contained in them, and do not exceed the thresholds established in the Royal Decree (RD)1481/2001, regulation based on the Directive 1999/31/EC on landfills [9, 10]. The management of both wastes implies high transport and storage costs, in addition to a potential environmental impact. For these reasons, this practice must be replaced by the valorisation of these wastes.

There are few studies in the literature about the characterization and valorisation of these wastes. Some authors report on the recovery of Cu and other marketable elements, such as Ag, Bi, Co and Zn [11–13]. Moreover, other authors have studied the removal/stabilization of hazardous elements, such As and Cd [14–16]. Other works suggest the recovery of high added-value elements, such as Ge and Se [17–19].

The properties of this type of residues depend not only on the composition of the concentrate fed into the FF, but also on temperature, oxidation conditions, which are determined by the furnace type, and the off-gas cleaning system employed [6, 15, 20]. For these reasons, it is necessary to characterize these residues before deciding the most suitable treatment, in order to recover the valuable elements [21–23].

Taking into account the previous facts, the main objective of this work was to propose an alternative process for the recovery of valuable elements contained in two wastes of a copper smelting plant (SC and SS), based on a thorough characterization.

2. Materials and methods

2.1 Materials

Four sampling campaigns were performed over a period of one month in March 2015. Four samples were collected for each of the previously commented wastes, i.e., sludges from scrubber (SS) and sludges from hydro-cyclones from CF off-gases (SC). At each sampling, about 4-5 kg for each sample was collected, and then they were dried at 60 °C and homogenized by manual agitation trying to break the clods but avoiding the breakage of particles the make up the sample. To verify the homogenization degree in some samples four aliquots were taken and measured by ICP-MS, finding that dispersion of the obtained concentrations was comparable to the RSD (Relative Standard Deviation) of the individual measurements. Moreover, some elements were measured by two different analytical techniques (ICP-MS and XRF), and the concentrations measured by both techniques were analogous. In addition, the SS samples were washed with distilled water to remove the remaining sulphuric acid, and it was verified that in the washing waters there was a negligible amount of the rest of the elements from the solid waste.

2.2. Characterization techniques

2.2.1. Granulometry

The particle size range of the samples was determined through a granulometric analysis using a modular analyser, Mastersizer 2000, with He-Ne laser diffraction technology at a wavelength of 632.8 nm. A representative amount of each sample was placed in ethanol and subjected to ultrasound for 10 minutes, followed by magnetic stirring for around 30 minutes. In addition, several certified reference materials were employed to calibrate the method: LTX3300C Nanosphere Size Standards, 2009A and 2009B Duke Polymer Microsphere Uniform Standards, 4009, 4009A and 4009B Duke Standards Microsphere Size Standards.

2.2.2. Mineralogy and Chemical composition

The study of the mineral phases present in the samples was performed using a Panalytical X'Pert Pro diffractometer, equipped with the Cu X-ray source and X'celerator detector, operating under the following conditions: voltage 40 kV; current 10 mA; range 5- 70 deg 2Θ; step size 0.017 deg 2Θ; time per step 50.165 s; divergence slit fixed, angle 0.5˚. The crystalline mineral fractions were identified using a X'Pert HighScore Plus software, along with the PDF-4 Minerals 2013 ICDD database. The quantification of the mineral phases was performed using the Rietveld method, which employs corundum as an internal standard to determine the amount of amorphous material. The X-ray diffraction analysis was carried out in Activation Laboratories (Actlabs) from Canada.

The major elements were identified and quantified by an X-ray fluorescence (XRF) analysis using a Panalytical (AXIOS model) sequential spectrometer. This system is equipped with an X-ray tube of 4 kW, Rh from window and anode, five analysing crystals (PX1, PE 002, LIF 200, Ge 111, and LIF 220) and two detectors (flow and scintillation). Previously, the samples were prepared as pressed discs of 40 mm in diameter and 25 mm in thickness.

The determination of trace elements was carried out by two measurement techniques: Inductively Coupled Plasma Mass Spectrometer (ICP-MS), Perkin Elmer Sciex ELAN 9000, and Inductively Coupled Plasma Optical Emission Spectrometry (ICP-OES), Varian 735 ES. Prior to the analysis, the samples were digested by mixing four acids (hydrochloric, nitric, perchloric and hydrofluoric acid). Moreover, some aliquots were dissolved by fusion with sodium peroxide.

133 *2.2.3. Thermal Analysis*

134 The thermal behaviour of the samples was studied by two methods: Thermogravimetric analysis (TGA)
135 and Differential Thermal analysis (DTA). A TG-85E 11 SDTA Mettler thermobalance was employed,
136 coupled to an ICP-MS equipment (Pffeifer ThermoStar) to determine the composition of off-gasses. The
137 operating conditions used were 25 – 1000 ˚C with a heating rate of 10 ˚C/min and an inert atmosphere of
138 N_2 with a flow of 50 mL/min.

139 *2.2.4. Scanning electron microscopy (SEM)*

140 The morphology and microstructure of the samples were studied using an environmental scanning electron
141 microscope QUANTA-Fei 200. This was equipped with an Energy Dispersive Spectrometer (EDS) which
142 enables multi-elemental semi-quantitative analysis. Then, a database was used to determine the
143 mineralogical composition [24].

144 A scanning electron microprobe (EPMA) JEOL JXA-820 model with four wavelength-dispersive X-ray
145 spectrometers and energy dispersive X-ray spectrometers (EDS) was used to obtain the spatial distribution
146 of several elements.

147 Prior to the analysis, the samples were inserted in the epoxy resin (Araldite®), then grinded with silicon
148 carbide paper (SIC paper) and polished with 6, 3 and 1 μm diamond paste. Afterwards, the samples were
149 covered with a thin layer of Au-Pd, in a Spark Blazer SCD 050, which made them conductive for electrons,
150 thus facilitating their observation in the microscope.

151 *2.2.5 Leaching test*

152 To evaluate the mobility of the pollutants, the UNE[1] leaching test [25], from Directive 1999/31/EC, was
153 applied. This directive regulates the disposal of waste by landfill. The waste acceptance criteria are
154 established for each type of landfill in this norm. The leaching test set out in the norm was adopted in this
155 experiment. The extraction fluid used was distilled water at a liquid/solid ratio of 10 L/kg (± 2%).
156 Polyethylene bottles were employed as extraction vessels, which were subjected to rotation with agitation

[1]Spanish acronym for “Una Norma Española”

157 equipment with Teflon-coated rod at 5-10 rpm during 24 ± 0.5 h. Then, the solution was vacuum filtered
158 using membrane filters of 0.45 μm pore size, in agreement with the UNE-EN 12457-4.

159 **3. Results and discussion**

160 **3.1 Physical-chemical characterization**

161 ***3.1.1. SS characterization***

162 *Granulometry*

163 The particle grain-size distribution is very useful to decide the possible applications and treatments of a
164 specific inorganic waste. The granulometry obtained for SS waste is summarised in Table S1, in
165 supplementary material. It is characterised by a high proportion of "silt" (87 ± 8 %), and low contents of
166 "clay" (11 ± 4 %) and "sand" particles (2.4 ± 1.3 %), presenting a monomodal distribution, as it is expected
167 from a wet precipitation process, with a maximum of 8 μm (Fig. 2a).

168 In the Fig. 2b the cumulative volume particles distribution curve is shown, where the percentiles can be
169 easily seen, obtaining that the median of the particles size distribution (d_{50}) is around 8 μm, and the d_{90} on
170 19 μm. This particle size distribution presents a high proportion of fine particles, which is highly beneficial
171 in the manufacturing of construction materials [26–29], or for improving the reactivity of the waste during
172 leaching processes [30, 31].

173

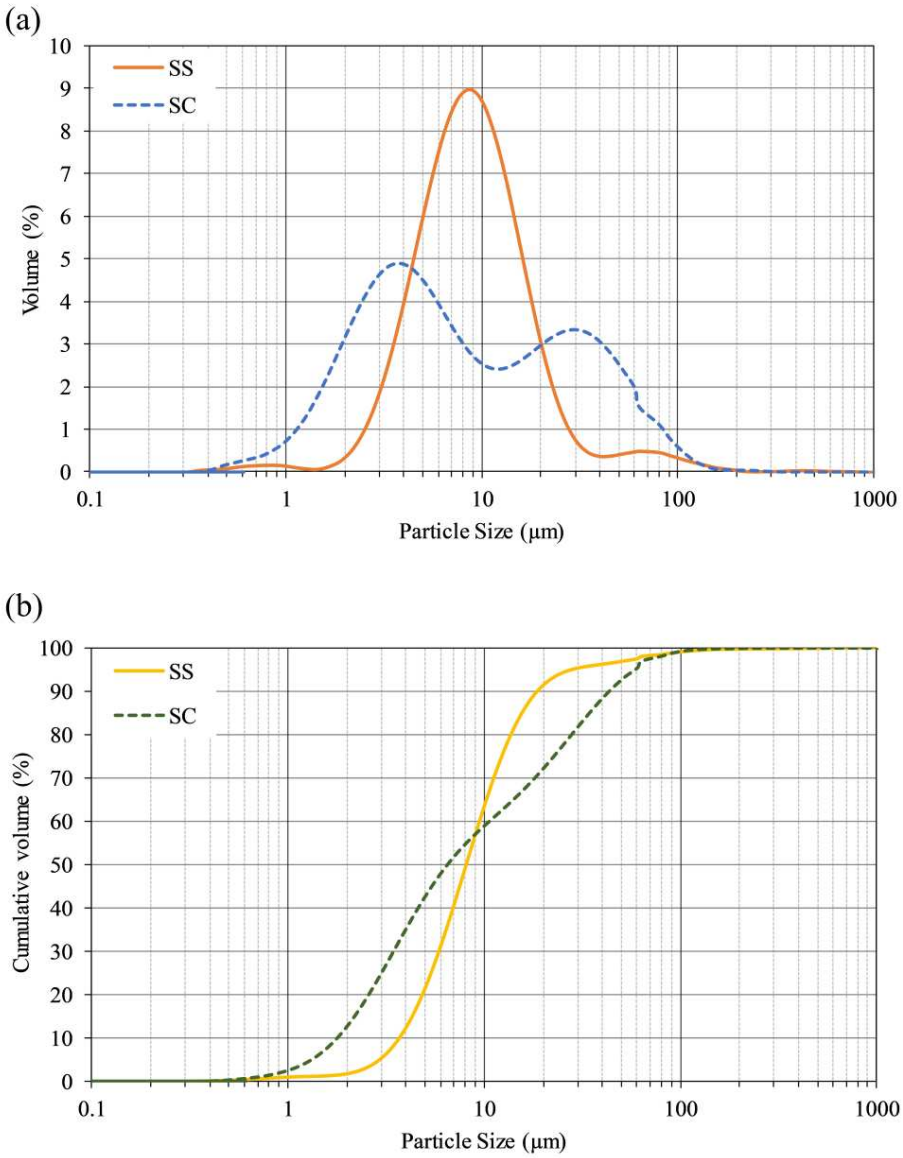

Fig. 2. Particle size distribution in % volume (a) and % cumulative volume (b) of the samples.

Elemental composition

The average concentration of the major and trace elements for the SS samples, measured by XRF and ICP-MS, are shown in Figures 3. This information is essential to identify the potential elements to be recovered and the pollutants that should be removed or reduced for their valorisation.

SS contains very high concentrations of Se (34.6 ± 0.4 %) and Pb (20.8 ± 0.3 %), whereas Hg (8.0 ± 0.1 %), S (6.3 ± 0.1 %), Sn (3.5 ± 0.1 %), Ge (2.0 ± 0.2 %) and I (1.4 ± 0.1 %) are in proportions less than 10 %. Other elements, such as As, Bi, Cu, Fe and Zn, were found in concentrations below 1 %, and Cr, Sb,

Te, Cd and Ni were found in trace concentrations (10-100 ppm). The high content of metals, such as Se, Pb, and Hg, could be due to the fact that they can be fully volatilized during smelting processes, after which they can either solidify as the gas cools down or form solid particles in the scrubber [6, 32].

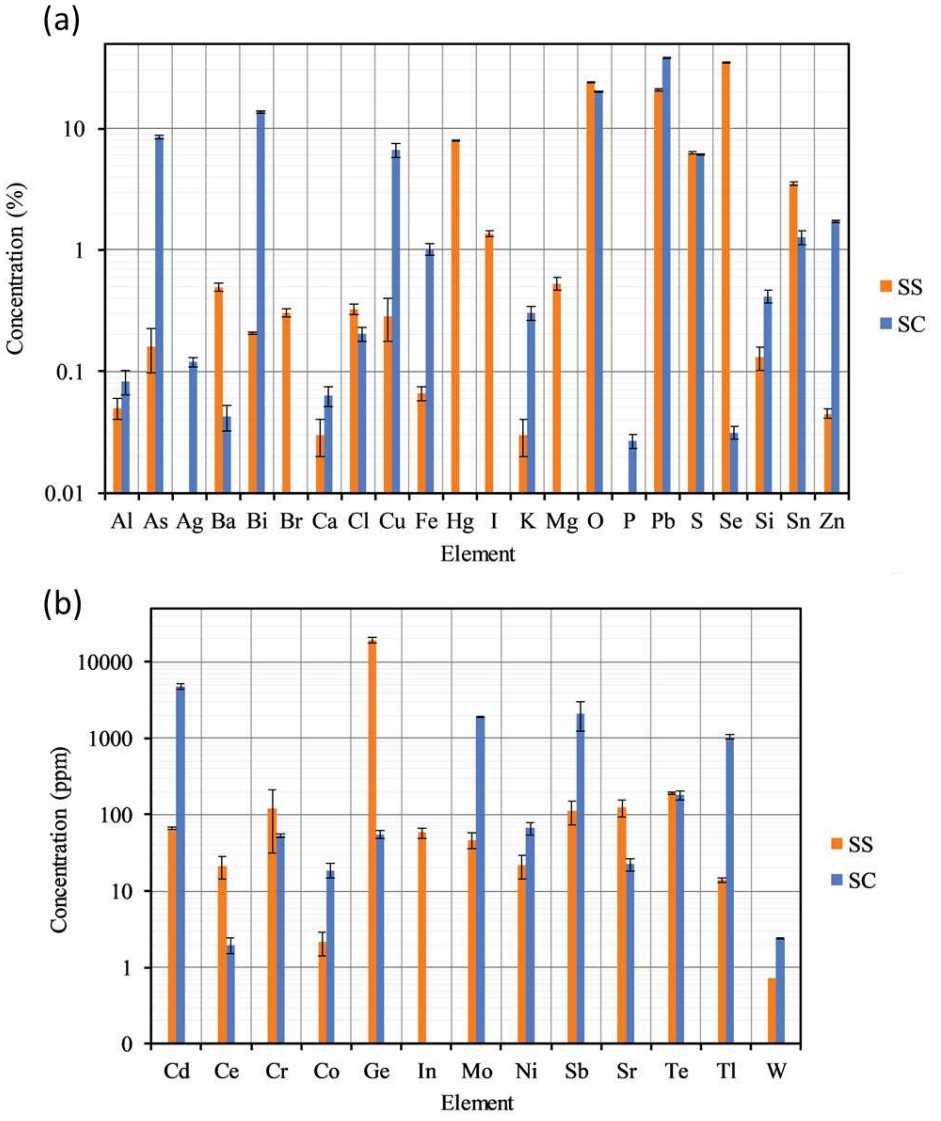

Fig. 3. Concentration of major elements (a) and trace elements (b) in the samples. The standard uncertainty (1 σ) was calculated as the standard deviation of the mean $\sigma = S_x / (n)^{1/2}$, where "n=3" is number of the samples.

Mineralogy

The Figure S1 shows the diffraction pattern (see, supplementary material). The main mineral phases were metallic selenium (34 % Se) and anglesite (27 % $PbSO_4$). According to the XRF results, the calculated $PbSO_4$ concentration (around 30%) is in agreement with the XRD one (experimental uncertainties ≤ 10 %). Therefore, both results agree with the content of Pb and Se obtained by XRF.

189 The metallic Se probably came from the reaction of SO_2 in the off-gas with SeO_2 volatized in the smelting
190 process and the water added in the gas scrubber system, as shown in reaction 1 [33].

$$SeO_{2\ (g)} + 2SO_{2(g)} + 2H_2O_{(l)} \rightarrow Se_{\ (s)} + 2H_2SO_{4(l)} \quad (1)$$

191 On the other hand, the $PbSO_4$ was probably formed during the cooling down of the off-gases, when the
192 solidified PbO reacts with SO_2 and O_2, according to reaction 2 [21, 34, 35]

$$PbO_{(s)} + SO_{2(g)} + 1/2\, O_{2\ (g)} \rightarrow PbSO_{4(s)} \quad (2)$$

193 In addition, SS had a high content of XRD-amorphous phase (around 40 %). The XRF analysis showed
194 high concentrations of other elements such as Hg, Sn and Ge, but no mineral phase was found associated
195 to them. Therefore, these elements have to be considered forming part of the XRD-amorphous phase, which
196 is formed by either no crystalline phases or microcrystalline phases, they cannot be detected by the XRD.
197 The formation of a high amorphous fraction can be due to the fast cooling produced in the gas scrubbing
198 [17, 21].

199 *Thermogravimetric analysis*

200 A TGA analysis was conducted to determine the thermal behaviour of the sludge (SS), contributing to the
201 identification of some chemical compounds that were present in the sample. The results can be seen in Fig.
202 4. It is observed that SS had three thermal events, which occurred at 310 ºC, 562 ºC and 730 ºC. SO_2 was
203 detected in the last two events, thus the mass losses were probably due to the decomposition of metal
204 sulphates. The sulphates decomposition is usually determined from the liberation of SO_3 but is decomposed
205 autocatalytically into SO_2 + O_2 in the plasm, being detected in the ICP-MS the m/z= 64 and m/z =32,
206 respectively.

207 The DTA curve shows a thermal event at 200 ºC, associated with the selenium melting. Then, it evaporated
208 at around 600 ºC [36, 37]. It can also be assumed that part of the mass loss (about 35 %) at 562ºC was due
209 to this evaporation. The transition temperatures obtained are slightly different than the average ones
210 obtained under ideal conditions for the transitions of Se (around 220°C and 685 °C), a fact being produced
211 by the interactions between the different substances that compose the real matrix.

212 The first thermal event at 310 ºC (DTG curve) corresponds to the decomposition of Hg_2SO_4 via the chemical
213 reaction 3 [38], which is in a proportion of 9 % in the sample taking into account the mass loss at this peak.
214 According to the stoichiometry of eq. 3, the reaction produces about 5 % of $HgSO_4$ that decompose at 562

ºC with other species ($Sn(SO_4)_2$, and Se volatilization) in accordance with reaction 4. In this point, the mass loss identified is about 44 %, being the remain loss mass about 7 % (from the total mass lost at 562 ºC, 51 %). This mass loss suggests that probably the sample also contains about 7 % $HgSO_4$, being in agreement to the Hg concentration measured by XRF.

$$Hg_2SO_{4(s)} \rightarrow HgSO_{4(s)} + Hg_{(g)} \quad (3)$$

$$HgSO_{4(s)} \rightarrow Hg_{(g)} + SO_{2(g)} + O_{2(g)} \quad (4)$$

In agreement with the XRF data the SS sample contains about 3.5 % Sn, which could be as $Sn(SO_4)_2$. The decomposition of $Sn(SO_4)_2$ occurred at around 580 °C, according to reaction 5 [38, 39]. It can also be assumed that part of the mass loss (about 5 %) at 562 °C was due to this decomposition, corresponding 9 % this compound in SS sample.

$$Sn(SO_4)_{2(s)} \rightarrow SnO_{2(s)} + 2SO_{3(g)} \quad (5)$$

The decomposition of $PbSO_4$ took place at probably 730 ºC, according to reaction 6 [39, 40]. In agreement with the mass loss, it is estimated that the sample contained around 23 % of this compound. This datum confirms the result obtained in the XRD analysis and the Pb obtained in the XRF analysis.

$$PbSO_{4(s)} \rightarrow PbO_{(s)} + SO_{3(g)} \quad (6)$$

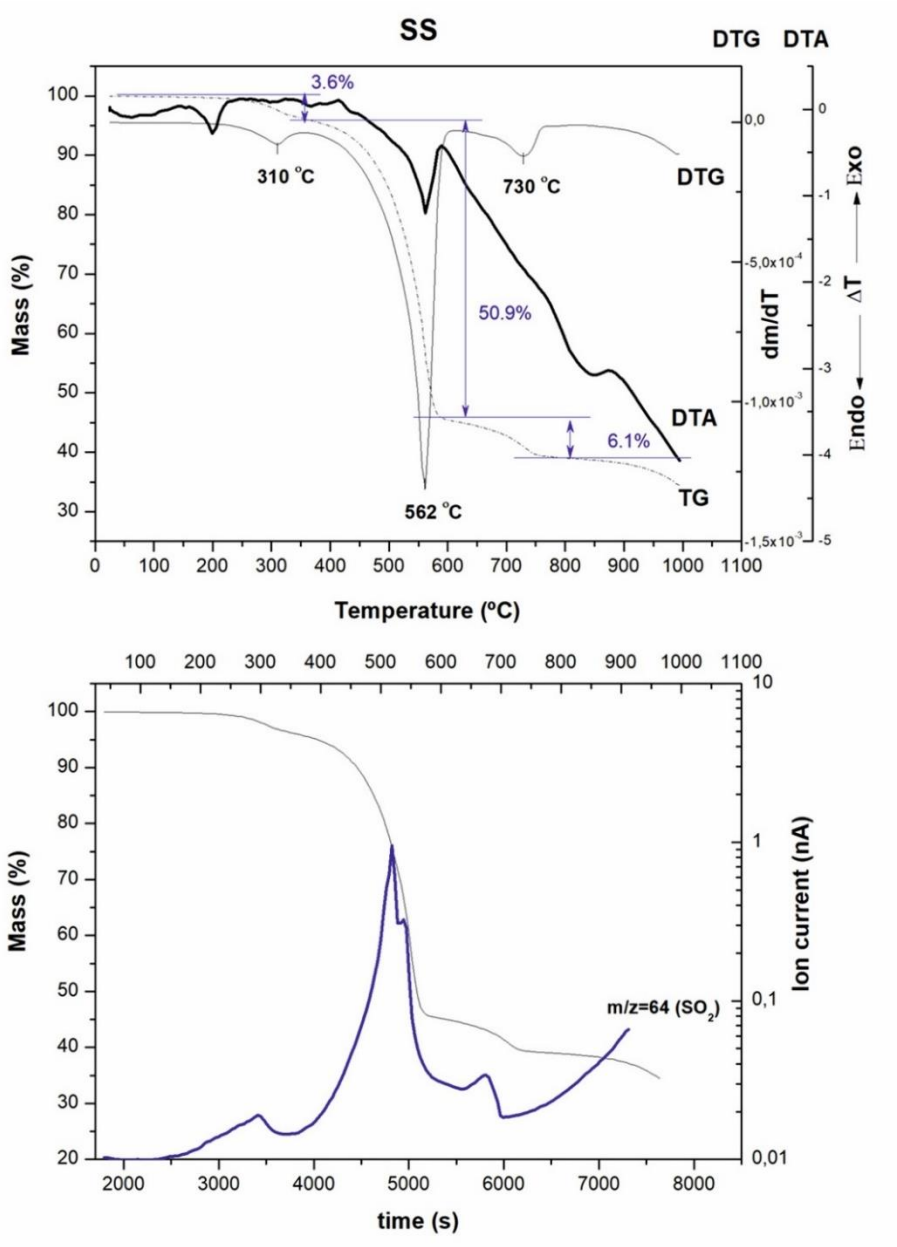

Fig. 4. TG-DTG-DTA curve and gases detected in the SS.

Scanning electron microscopy (SEM)

The SEM analysis performs a visual study of the surface of the residue, which can help to the identify pollutant or unknown particles, thus providing information about the interactions between the phases present in the material. In addition, this technique is used for the determination of the size, texture and morphology of the particles in order to understand the micro-properties of the material. The data obtained in the SEM and EDS analyses of the SS sample are shown in Fig. 5.

The sample presents an agglomerated morphology formed by fine particles, according to the granulometric analysis. The main composition determined by EDS is similar to that obtained in the XRF results, in which the sample was mainly composed of Se, Pb, Hg and S. Due to their amorphous morphology, it was difficult to identify the compounds that are presented in the fine fraction. However, it was possible to identify large particles (point 1, Fig. 5), which had a high content of Pb, S and O, in agreement with the EDS spectra. Their composition and prismatic habit suggest that these particles are composed of lead sulphate (anglesite), with a size between 1 and 50 μm. Furthermore, the experimental mass ratio Pb/S is 6.17, which is in agreement with the theoretical ratio of anglesite (Pb/S = 6.18), within of experimental uncertainties (≤ 10 %). This result agrees with the previous results that one of the mineral phases found in the sample was anglesite ($PbSO_4$).

Dark grey particles were also detected (point 2, Fig. 5), with a Si/O mass ratio analogous to quartz (SiO_2), but its characteristic crystalline habit was not observed. The sample present around 0.2 % of this compound, proving the presence of Si in the sample.

In addition, it was identified small particles of metallic Se (point 3, Fig. 5), which presented a granular shape with a size between 2 and 5 μm. These results are in line with those obtained in the XRD analysis. Moreover, medium-sized particles were found (point 4, Fig. 5), whose S and Cu proportion was like that of covellite (CuS). The sample contained less than 1 % of this compound. It can also be seen that its texture was granular, with a size of around 20 μm. This result confirms the presence of Cu in the sample, in agreement with the data obtained in the XRF analysis.

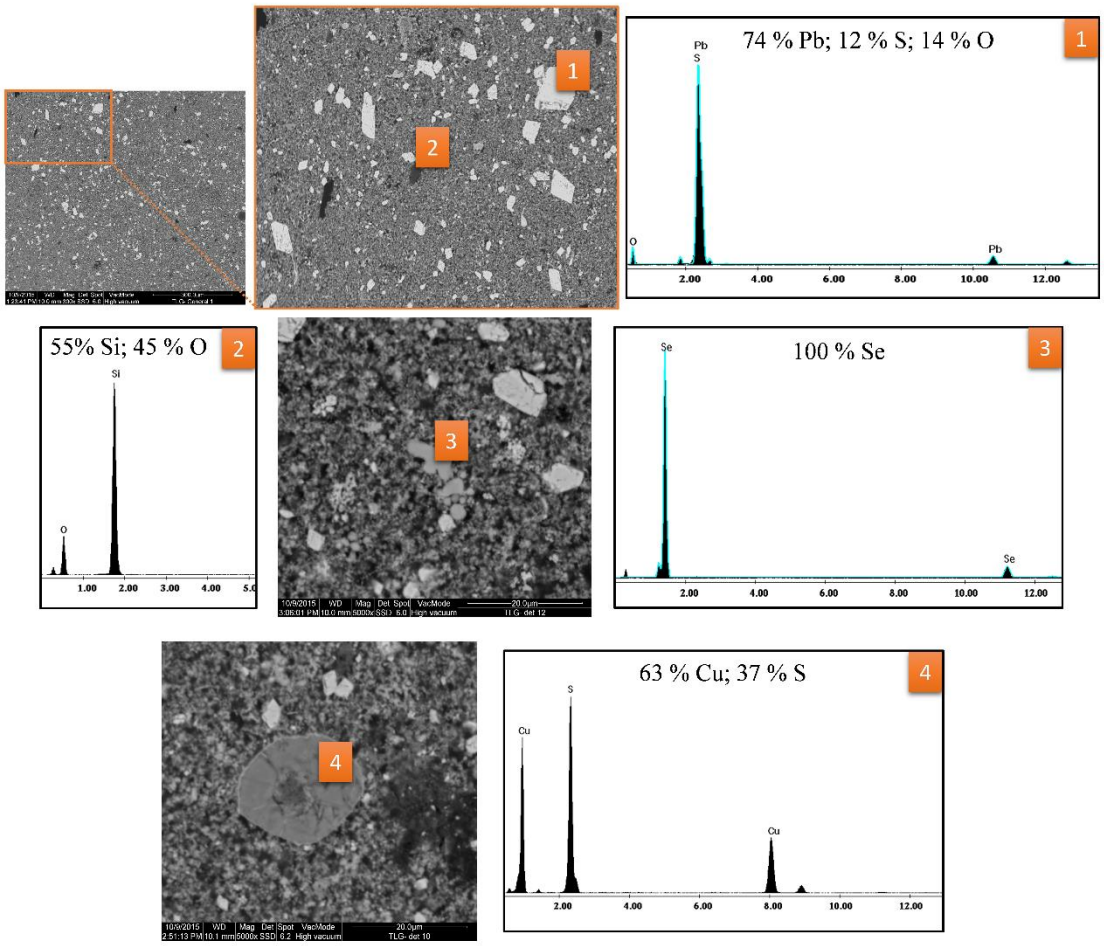

Elements	Cl	Cu	Ge	Hg	I	O	Pb	S	Se
% Wt	0.9	0.7	0.5	11	2.4	10	22	7.4	45

Fig. 5. Scanning electron micrograph of SS particles. The table also shows the general composition determined by EDS from the image located at the top left.

252

253 The secondary electron image of the SS region and X-ray mapping of principal elements (Se, Pb, S, Hg,
254 As, Cu, Sn and Cd) present in the sample are shown in Fig S2 (see, supplementary material). Se, Hg, As,
255 Sn and Cd were distributed throughout the matrix. It is observed that there are regions in which Pb, and S
256 are coincident, proving the existence of a $PbSO_4$ phase. Moreover, there were areas identified in which Cu
257 and S were coincident, confirming the presence of CuS previously found in the SEM analysis.

258 *Leaching test*

259 A UNE leaching test [25] was carried out, according to the RD 1481/2001 of 27 December, which regulates
260 the disposal of waste by landfill, in agreement with the provisions of Directive 1999/31/EC on landfills.

261 Table 1 shows the results obtained and the threshold concentration for non-hazardous material and
262 hazardous material, expressed in mg of element leached per kg of original material. The transfer coefficients
263 (η) are also shown, which represent the fraction of an element (%) that has been transferred into the liquid.

264 The SS leached a concentration (C_{SS}) of As, Cd, Cu, S, Pb, Sb and Zn that exceeded the thresholds
265 established for their disposal as non-hazardous material in a controlled landfill. Moreover, the SS matrix
266 leached 99 % As, 96 % S, 63 % Cd, 53 % Cu and 43 % Zn, whereas the Pb leached was below 0.01. The
267 transfer into the solution of sulphur (as anion SO_4^{2-}) is much higher than some heavy metals (e.g., Pb
268 presents a transfer very low, around 0.01%). This is due to metals such as Pb, Sn, Fe, etc., which form very
269 "reactive" chemical species with a high tendency to be bound onto the solid material. The amount of each
270 metal precipitated will depend on its mobility into the leaching solution. These results are in line with other
271 studies where metals, such as Pb, present a low mobility in water [41–43].

272 A leaching test determined that this waste is likely to produce leachates with high contents of pollutants,
273 which could be harmful to human health and the environment in the case of their disposal by landfill.
274 Therefore, other alternatives must be sought, which focus on obtaining not only health and environmental
275 benefits, but also economic solutions.

Element	**C_{SS} (mg/kg)**	**η_{SS} (%)**	**C_{SC} (mg/kg)**	**η_{SC} (%)**	**Threshold Level Non-Hazardous Material (mg/kg)**	**Threshold Level Hazardous Material (mg/kg)**
As	1579	99	222	$2.6 \cdot 10^{-1}$	2	25
Ba	< 0.02	-	< 0.02	-	100	300
Cd	41.7	63	1410	29	1	5
Co	0.19	10	1.2	6	-	-
Cr	2.3	1.9	< 0.02	-	10	70
Cu	1525	53	11093	16	50	100
Fe	295	44	0.4	$3.9 \cdot 10^{-3}$	-	-
Mo	2.93	6.2	1.1	$5.6 \cdot 10^{-2}$	10	30
Ni	4.39	20	7.1	11	10	40
Pb	19	$9.1 \cdot 10^{-3}$	20	$5.2 \cdot 10^{-3}$	10	50
S	60160	96	12880	21	20000	50000
Sb	2.7	2.4	5.7	$2.7 \cdot 10^{-1}$	0.7	5
Se	< 0.02	-	0.4	$1.3 \cdot 10^{-1}$	0.5	7
Sn	12.4	$3.5 \cdot 10^{-2}$	< 0.01	-	-	-
Tl	2.4	17	114	11	-	-
Zn	205	43	14594	85	50	200

Table 1. UNE test results for the samples.

276

3.1.2. SC characterization

Granulometry

The particle size distribution (% volume) obtained for SC is compiled in Table S1. The SC sample is composed of a high concentration of "silt" particles (62 ± 3 %), followed by a proportion of "clay" particles (34 ± 3 %) and a low content of "sand" particles (4.6 ± 1.5 %), presenting a multimodal size distribution with two maximums at 4 and 30 μm (Fig. 2a). The second maximum could be also linked to the hydro-cyclones efficiency, which could not be 100 %, thus coarse particles may be found in this waste.

The Fig. 2b shows the cumulative volume particles size distribution obtained for SC, in which is observed that the median particles size distribution (d_{50}) is about 6.5 μm and d_{90} on 42 μm. As was previously mentioned, the fine particles (especially those between 8-40 μm), are very beneficial for construction materials manufacturing, since by controlling the size particle of the cement components can be also optimized some of its properties related to the setting, hardening and curing, as the compressive strength or permeability [26, 28, 29, 44]. In addition, the recovery by hydrometallurgy route can be also favoured due to the high reactivity of fine particles, lower than 40 μm (greater specific area) [30, 31].

Elemental composition

The average composition of the major and trace elements for SC is shown in Fig. 3. The SC sample contained Pb (38 ± 1 %) as the major element, and in lower proportion Bi (13.6 ± 0.4 %), As (8.5 ± 0.3 %), Cu (6.7 ± 0.9 %), S (6.1 ± 0.1 %), Zn (1.7 ± 0.1 %) and Sn (1.3 ± 0.2 %). Other elements, such as Ag, K, Fe and Si, were found in a proportion below 1 %. Furthermore, the sample presented Cd, Mo, Sb and Tl (5000-2000 ppm), and Te, Ni, Ge and Cr (200-50 ppm) as their main trace elements.

The Cu present in this waste came from the converter furnace's off-gases, which carry substantial levels of dust, composing particles of unreacted concentrate and droplets of matte/slag. These dusts generally contain 20-40 % mass Cu at the converters output [6]. Consequently, most of these dusts were recovered in the electrostatic filters and the hydro-cyclones and then they were recycled in the FF, returning around 80 % Cu. On the other hand, the fine dust (SC) contained a low Cu concentration and was rich in impurities, such as Pb, As, Bi and Zn, which were volatilized in the smelting process and precipitated as the gases cool down [15, 32], in agreement with the results obtained.

Mineralogy

From the SC diffractogram (Fig. S1), the anglesite (32 % $PbSO_4$) was the only mineral phase identified. Lead sulphate was formed during the condensation of Pb volatilized with $SO_2 + O_2$ by reaction 2 [21, 22, 35]. In agreement with the literature consulted [6, 21, 32] and the XRF analysis, other crystalline phases should be identified, but it should be noted the waste is a sludge composed of fine particles of converted dust come from hydro-cyclones, in which the most oxides react with diluted sulphuric acid solution becoming in sulphates, that they are not detected by XRD.

Furthermore, SC had a high content of XRD-amorphous phase (about 68 %). The XRF analysis showed a high concentration of As, Bi, Cu and Sn, but no mineral phases of these were identified by XRD, suggesting this fact that they are found in the called amorphous phase, which could contain these elements either as a poorly crystalline phase or other microcrystalline phases, which cannot be detected by the equipment. The formation of a large amorphous fraction can be due to a short cooling time in the gas cleaning system [17, 21].

Thermogravimetric analysis

In Fig. 6, the DTA curve reveals that the most thermal events were endothermic and indicated the decomposition of chemical species contained in the matrix. The SC sample had seven thermal events, which occurred at 108 ºC, 290 ºC, 415 ºC, 446 ºC, 563 ºC, 660 ºC and 782 ºC. Water was detected in the first and second events, which were due to a loss of crystallised water of some hydrated compound. The third thermal event was exothermic, which are probably associated with some chemical and physical thermal reaction types [45]. The other thermal events were due to the decomposition of sulphates, corroborated by the detection of SO_2 in the ICP-MS system.

According to the decomposition temperature and the total loss of water, the hydrated compound could be a copper (II) sulphate pentahydrate ($CuSO_4 \cdot 5H_2O$) which is dehydrated at 108 ºC and 290 ºC, according to reaction 7 and 8, and then is decomposed at 446 ºC, following reactions 9. The literature consulted [45–48] confirms that the dehydrated copper sulphate gives three thermal events, which were detected around 75 °C, 110 °C and 250 °C, however, the water loss was detected in the first two thermal events in the range 50 -300 ºC, which can be due to the interactions between the different substances that compose the matrix and/or experimental conditions (heating rate). Considering the mass loss, it is estimated that the sample

contained around 6 % of this compound. However, Cu concentration in the matrix was much higher (about 7 %), meaning that Cu was forming other compounds.

$$CuSO_4 \cdot 5H_2O_{(s)} \rightarrow CuSO_4 \cdot H_2O_{(s)} + 4H_2O_{(g)} \quad (108\ ºC) \tag{7}$$

$$CuSO_4 \cdot H_2O_{(s)} \rightarrow CuSO_{4\,(s)} + H_2O_{(g)} \quad (290\ ºC) \tag{8}$$

$$CuSO_{4(s)} \rightarrow CuO_{(s)} + SO_{3(g)} \quad (446\ ºC) \tag{9}$$

The thermal event at 415 ºC probably corresponds to thermal oxidation of CuS to Cu_2S, according to reaction 10 [45, 49]. However, it was not possible to calculate the CuS concentration in the sample due to SO_2 liberated in this event detected together with the SO_2 generated in the $CuSO_4$ decomposition. Moreover, the loss mass was not significant (see curve TG, Fig 9).

$$2CuS_{(s)} + O_{2(g)} \rightarrow Cu_2S_{(s)} + SO_{2(g)} \tag{10}$$

The decomposition of iron (II) sulphate ($FeSO_4$) occurred at 563ºC [45, 50]. According to the amount of mass lost, it was calculated that the sample contained around 3 % of this compound. This result confirms that the Fe concentration obtained in the XRF analysis (around 1 %) is in line with the content of $FeSO_4$ in the sample.

$$FeSO_{4(s)} \rightarrow FeO_{(s)} + SO_{3(g)} \tag{11}$$

The mass loss at 660 ºC corresponds to the decomposition of $ZnSO_4$, according to reaction 12 [39, 46, 50]. Considering the mass loss, it is estimated that the sample had about 5 % $ZnSO_4$. This datum is in line with the percentage of Zn found in the XRF analysis (around 2 %).

$$ZnSO_{4(s)} \rightarrow ZnO_{(s)} + SO_{3(g)} \tag{12}$$

The mass loss produced at 782 ºC is associated with the thermal decomposition of anglesite ($PbSO_4$), according to reaction 6 [39, 40]. The percent mass loss, about 8 %, suggests that the sample contained 30 % anglesite. This result is in line with those obtained in the XRD and XRF analyses.

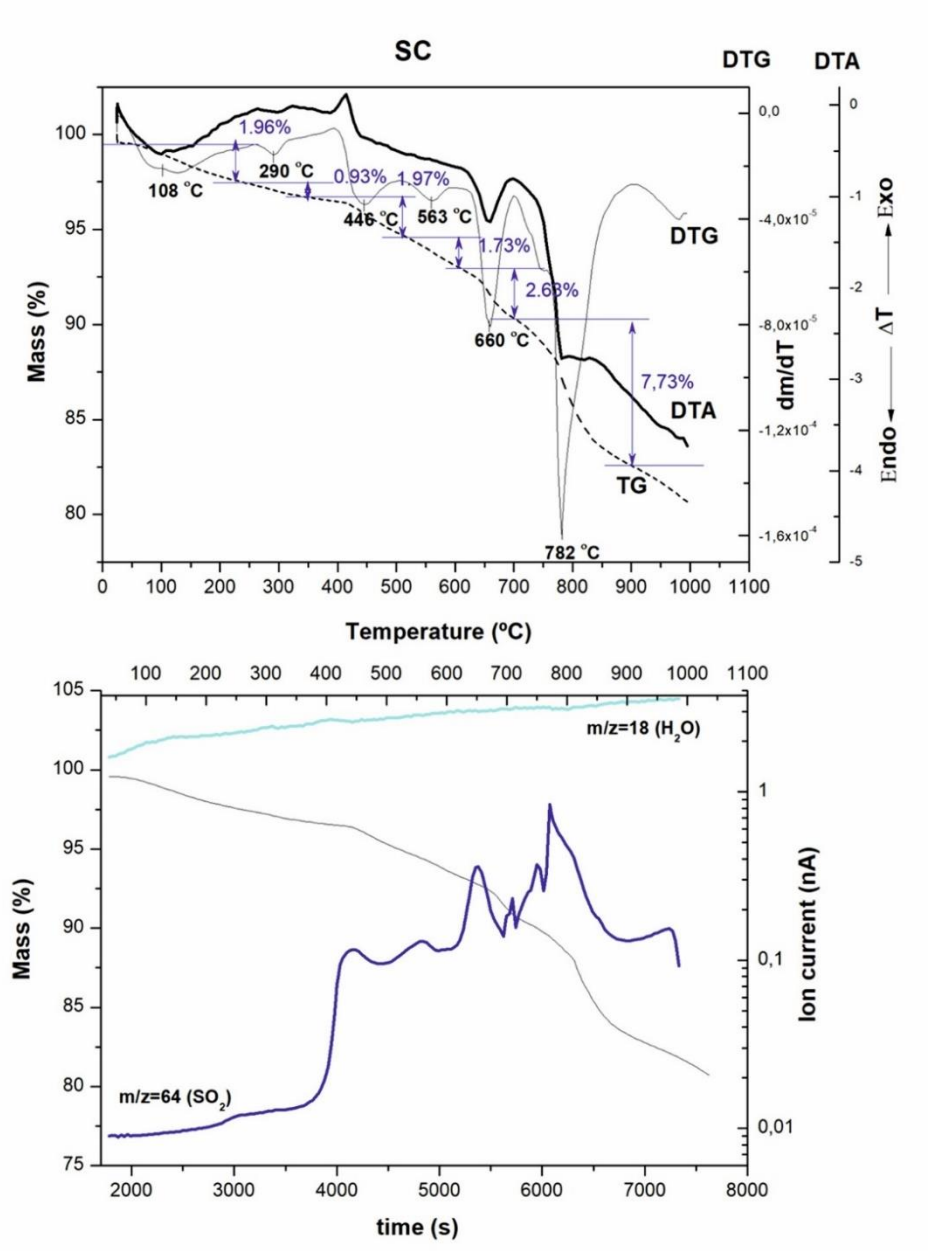

Fig. 6. TG-DTG-DTA curve and gases detected in the SC.

Scanning electron microscopy

The SEM and EDS analyses of SC determined that sample was composed of agglomerates of very fine particles with the inclusion of spherical particles with size between 20-50 μm (see, Fig. 7), in agreement with the granulometry results. These spherical particles (point 1, Fig. 7) had a high concentration of Cu and S (around 74 % and 23 %, respectively) according to the EDS spectra. Their composition and morphology suggest that these particles are similar to chalcocite in composition (Cu_2S). This chemical species was not detected in the thermal analysis since the decomposition of Cu_2S occurs at a higher temperature (> 1100 ºC). Moreover, the presence of these particles and the CuS, detected in the thermal analysis, confirm that

Cu was found as sulphides and sulphates in this sludge [17, 21]. According to the results obtained in the TGA analysis, and considering the Cu concentration, it is estimated that the SC contained about 4 % of this compound. Moreover, it was proved that bright particles (point 2, Fig. 7) were composed by Pb, S and O in the same proportion that to the one found in lead sulphates (anglesite). This mineral phase was also identified in the XRD and TGA analyses. This mineral showed several crystalline habits; in this case, it can be observed that a small crystal with a laminar texture is involved. The composition of the grey areas (area 3, Fig. 7) was analogous to the general composition determined by the EDS and XRF analyses (table, Fig. 7), thus that it can be asserted that the matrix was composed of fine particle aggregates.

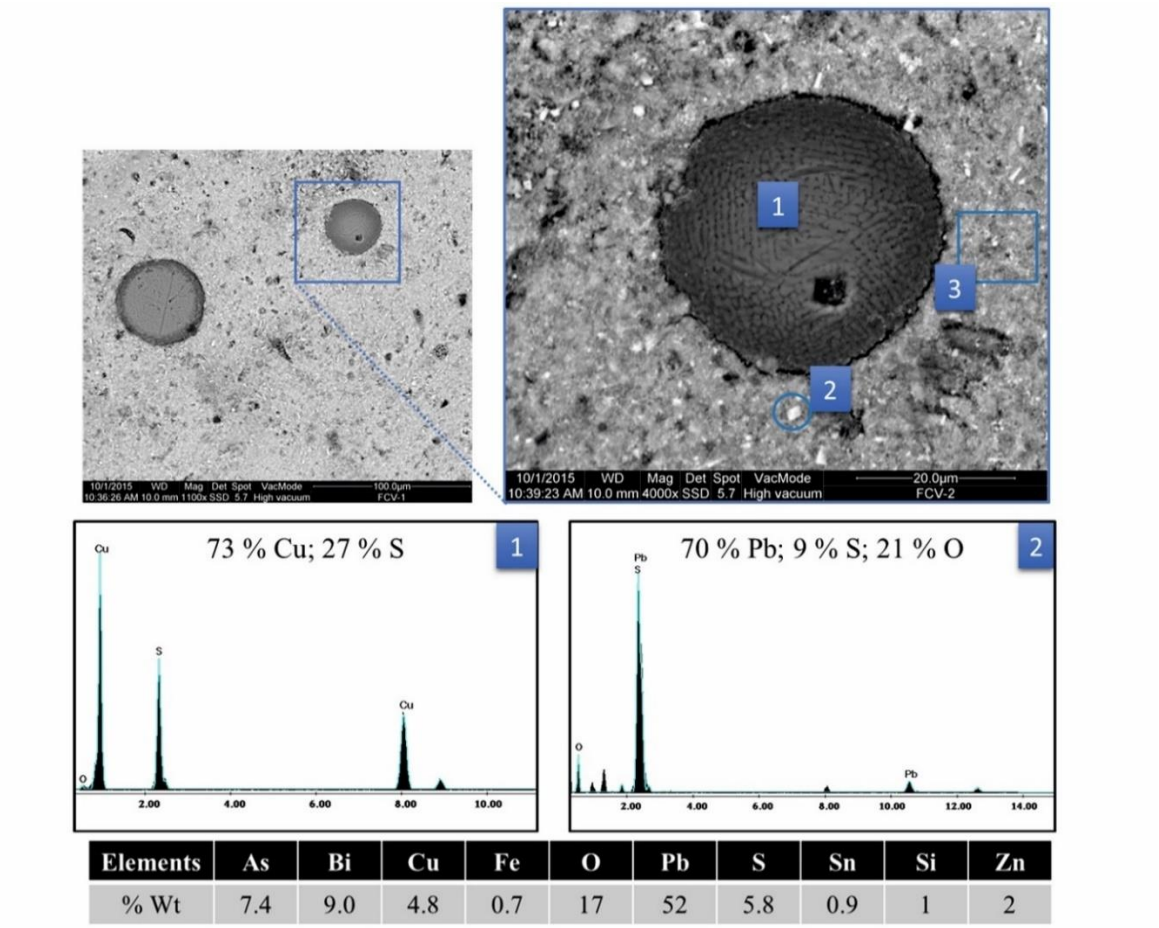

Elements	As	Bi	Cu	Fe	O	Pb	S	Sn	Si	Zn
% Wt	7.4	9.0	4.8	0.7	17	52	5.8	0.9	1	2

Fig. 7. Scanning electron micrograph of SC particles and general composition determined by EDS.

The distribution of principal elements (Pb, Bi, As, Cu, S, Zn, Sn and Fe) present in the sample is shown in Fig. S3, which includes a secondary electron image and X-ray mapping of a SC region. As can be observed, Pb, Bi, As, S, and Sn are uniformly distributed in the sample. Moreover, this image confirms the presence

368 of As and Bi in the amorphous phase, which was not detected in the XRD or SEM analyses. Both elements
369 could be present as oxide [15, 21, 51]

370 The mapping reveals regions with a high content of sulphur and copper, which corresponds to the spherical
371 particles previously identified as Cu_2S in the SEM analysis. Moreover, there were sections in which sulphur
372 and zinc coincided, confirming the presence of $ZnSO_4$, previously found in the results of the TGA analysis.
373 Likewise, there were also areas where iron and sulphur were coincident, confirming the presence of $FeSO_4$,
374 which was also identified in the TGA analysis.

375 *Leaching*

376 The SC sample leached a concentration (C_{SC}) of As, Cd, Cu, Pb, Sb and Zn above the limit established for
377 its landfill disposal as a non-hazardous material (Table 1). This matrix leached 85 % Zn, 29 % Cd, 21 % S
378 and 16 % Cu, whereas the amount of Sb and Pb leached were below 1 % and 0.01 %, respectively. This
379 waste tends to produce leachates with a high content of pollutants, consequently the residue must be
380 stabilized prior to its disposal by landfill or its new application, suggesting the study of alternative
381 treatments to develop health, environmental and economic benefits.

382 **3.2. Discussion**

383 These waste (SS and SC) presented particles size with a median (d_{50}) around 10 μm, which can be highly
384 beneficial in the manufacturing of construction materials [25–28] and can also favour the recovery of some
385 metals during the hydrometallurgy route due to the high reactivity of the fine particles in view of their
386 greater specific area [29, 30].

387 The elemental composition confirms that both residues are different even though both contain Pb as one of
388 their major elements. The high Pb concentration is due to the fact that around 50 % of Pb, which is present
389 in copper ore concentrate, is volatilized during the FF and CF processes [6, 52]. Anglesite ($PbSO_4$) is the
390 dominant mineral phase present in both wastes (see, Fig. S1), at 27 % and 33 % for SS and SC, respectively,
391 in agreement with the high contents of lead in these samples. The SEM images (see, Fig. 5 and 7) reveal
392 that the size particle of $PbSO_4$ (anglesite) is different, which is probably associated with different formation
393 mechanisms. The size of $PbSO_4$ particles in SS is larger than in SC. The small lead sulphate particles are
394 apparently formed throughout the fast cooling from CF off-gases. On the other hand, the large particles are

probably formed when the remaining particles of PbO from off-gases of FF and CF react with sulphuric acid diluted in the scrubber section.

The main difference between the two wastes is the high content of metallic selenium (around 35 % Se) in SS, which probably comes from CF gases, since around 25 % of Se is volatilized in CF, whereas 5 % is volatilized in FF [6, 32].

Both wastes contain high concentrations of XRD-amorphous phase, approximately 40 % in SS and 68 % in SC. Some compounds present in the XRD-amorphous phase of SS and SC were identified by thermogravimetric and SEM-EDS analysis. SC contains copper, iron, lead and zinc sulphates ($CuSO_4 \cdot 5H_2O$, $FeSO_4$, and $ZnSO_4$) formed from the oxides during the cooling and cleaning steps of the gas. Copper sulphurs (CuS and Cu_2S), were also found, probably coming from droplets of matte carried in the off-gas that solidified unreacted during cooling gas. The high Cu concentration in SC samples demonstrates that 80 % of the Cu present in the converter dusts is recovered by the hydro-cyclones. In addition, the amorphous material of SS is composed of mercury and tin sulphates (Hg_2SO_4, $HgSO_4$ and $Sn(SO_4)_2$), which probably is produced the reaction of both Sn and Hg oxides with diluted sulphuric acid in the scrubber section. Finally, the fine particles of CuS found in SEM-EDS analysis have the same origin as mentioned above. The SiO_2 was also found in the SS sample, which likely comes from small particles of unreacted flux.

Another difference between these two residues is the concentration of impurities such as As, Bi, Cd, Sb and Zn. The low concentration of impurities such as As, Bi and Sb in SS was found due to the most of them are removed in the electrostatic filters before the gases are sent to the scrubbing section. On the other hand, SC has a high content of As, Bi, Cd, Sb and Zn, since this residue is formed by fine particles coming from converters dust, since it contains the major impurities levels. The SC sample contains a high concentration of As and Bi (around 10 %), however, no compound these elements were found neither by XRD, SEM or thermal analysis. Considering the consulted literature, these elements could be as oxides (As_2O_3 and Bi_2O_3) [6, 23, 32, 51, 53]. Furthermore, the SS sample present around 2 % Ge which could be as GeO and/or GeS_2 [18], but these compounds were also not detected by the previous characterization techniques.

A summary of the physicochemical characterization performed in both wastes (SS and SC) is shown in Table 2.

	SS			***SC***		
Granulometry	clay	silt	sand	clay	silt	sand
	11	87	2	34	62	4
	Element (%)	Compound	Mineral	Element (%)	Compound	Mineral
As	0.16	N.I	N.I	8.5	N.I	N.I
Bi	0.21	N.I	N.I	14	N.I	N.I
Cu	0.30	CuS (0.5 %)	N.I	7.0	$CuSO_4 \cdot 5H_2O$ (6 %) CuS* Cu_2S (4 %)	N.I
Fe	0.07	N.I	N.I	1.0	$FeSO_4$ (3 %)	N.I
Hg	8.0	Hg_2SO_4 (5%) $HgSO_4$ (7%)	N.I	< 0.01	N.I	N.I
Pb	21	N.I	$PbSO_4$ (27 %)	38	N.I	$PbSO_4$ (32 %)
Se	35	N.I	Se (34 %)	0.03	N.I	N.I
Si	0.13	SiO_2 (0.2 %)	N.I	0.42	N.I	N.I
Sn	3.5	$Sn(SO_4)_2$ (9%)	N.I	1.3	N.I	N.I
Zn	0.05	N.I	N.I	1.7	$ZnSO_4$ (5 %)	N.I

Table 2. *Summary of the components found in the SS and SC samples and the granulometry analysis. N.I= Not Identified.*

**No possible to calculate the CuS concentration in SS due to SO_2 liberated in this event is detected together with the SO_2 generated in the $CuSO_4$ decomposition*

The content of valuable metals in both wastes (SC and SS) along with the increasing cost of waste disposal on controlled landfill, increasingly restrictive legislation and their potential risk to human health and the environment, suggest that efforts should be focused on valorising these wastes. Taking into account the physical, chemical and mineralogy characterization and the consulted bibliographic, these residues could be an important secondary source of Se and Pb [15, 19, 32, 54–56]. The recovery of these as metals with 99.99% purity is proposed, in order to make higher profits and thus contributing to the circular economy of these elements in the copper production process.

3.3. Proposal for their valorisation

Currently, there are not any companies which use these kinds of wastes as a secondary source of Se and Pb. Copper anode slime is the main source of selenium, since there are no mineral reserves. There are several processes that nowadays are being applied at copper refineries whose advantages and disadvantages

436 are summarised in Table S2 [37, 54–58]. On the other hand, Pb is usually extracted together with Zn from
437 the dust generated in an electric furnace, which is one of the main secondary sources of Pb [22, 59–62].

438 The metal global demand will increase in the next decades, including Pb and Se, due to using wind, solar,
439 and energy storage batteries and new technologies [63, 64]. Nowadays, selenium is marketed as selenium
440 metal, with different refined grades, or selenium dioxide. The metal Se price is around $4.4 \cdot 10^4$ \$/t [65],
441 being above the copper ($6.2 \cdot 10^3$ \$/t). The Pb is consumed as lead metal with a price around $1.9 \cdot 10^3$ \$/t,
442 depending of refined grade [65, 66]. Therefore, the recovery of Se and Pb involves an associated value,
443 which can contribute considerably to the economic viability of the activity which will mainly depend on
444 manufacturing cost.

445 There are different routes for the metal recovery, as such pyrometallurgy, hydrometallurgy or a combination
446 of both. The recovery path will depend on many factors, such as the physical, chemical and mineralogical
447 characteristics of wastes, their quantity generated (40 t/y of SS and 430 t/y of SC), the production costs and
448 potential environmental impacts. In the present study, it has been proposed to apply the pyro-
449 hydrometallurgical route for recovery Se and Pb, based on the chemical composition and physicochemical
450 properties of the wastes, which could satisfy the requirements of smelting for the suitable use of these
451 residues as a secondary source in the appropriate environmental conditions.

452 The process would begin with the recovery of selenium from SS using a roasting process [37, 56, 58, 67],
453 being separated due to the existence of different boiling points in relation to the other components of the
454 waste, as was verified by the TGA analysis. The process involves the roasting of SS at 700 ºC and then, a
455 cooling process in two steps. In the first cooling step, the mercury species would be removed from the off-
456 gases using a condenser [68], in which the gases are cooled down to around 300 ºC (below to evaporation
457 point of Hg), obtaining a solid residue from the process. In the second step, the metallic Se is recovered at
458 a lower temperature; lower to Se melting point, 221 ºC, as indicated in DTA curve. The flowchart proposed
459 for the valorisation of these wastes is shown in Fig 8.

460 The process would continue with the blending of the calcined Pb-rich residue with SC to recover lead by
461 hydrometallurgical route [17, 19, 61, 69]. The stages would begin with Pb extraction using a sodium
462 hydroxide solution (NaOH), since sulphate lead is dissolved easily and selectively in that leaching media
463 [70, 71]. Then, the obtained solution would be separate from the solid residue, which would be mainly
464 compose of Cu, As, Bi and other elements, for instance, Ge. Afterwards, it is proposed the recovery of

metallic Pb from the solution through a cementation process, by adding Zn powder, and the final solution could be recycled to the leaching process. This practice is widely used in another industrial hydrometallurgy processes [70, 72, 73].

Currently, the generation of these two wastes imply the management of a total of 450 t/y of hazardous material. The proposed process could produce about 13.6 t/y of metallic Se and around 171 t/y of metallic Pb with high purity, minimizing one half the amount of these wastes. This fact would reduce the management waste costs and, in addition, could result in a significant revenue gains, as a result of the sale of these metals that it could reach more than $9.0 \cdot 10^5$ *$/y*. This proposal could be feasible, however, provided it is thoroughly studied and quantified, with the aim of evaluating their technical, environmental and economic viability.

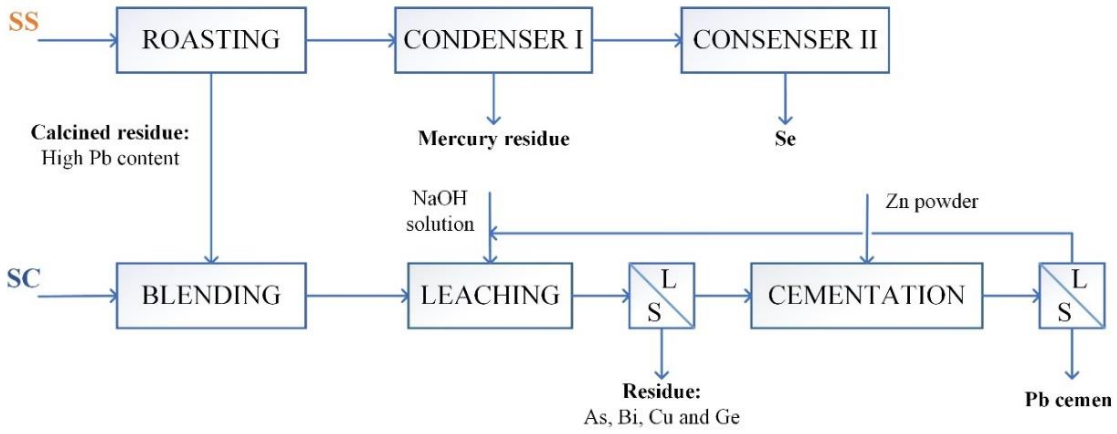

Fig. 8. Flowchart of the SS and SC treatment proposed.

4. Conclusions

The present work is focused on finding and designing the most appropriate application and treatment for the valorisation of two wastes coming from the gas cleaning system of the smelting and converting furnaces belonging to a pyrometallurgical plant. For that, a deep physicochemical characterization of them was previously carried out. From this study, it is concluded that:

a. Both wastes are mainly composed of fine particles (< 10 µm), which is highly beneficial in the proposed hydrometallurgy process.
b. SS and SC wastes have a high Pb content, around 21 % and 38 %, respectively, which is mainly present as anglesite ($PbSO_4$).

c. SS also contains a high Se concentration (~ 34 %) as metallic selenium, and, in addition, this sludge presents high levels of Hg (~ 8 %) and Sn (~ 4%) as sulphates (Hg_2SO_4, $HgSO_4$ and $Sn(SO_4)_2$, respectively).

d. SC contains Cu (~ 7 %), which is found as CuS, Cu_2S and $CuSO_4{\cdot}5H_2O$. Moreover, SC presents a high content of As and Bi (~ 10 %), but no compounds of these elements were identified.

e. Both wastes are considered hazardous materials, since they can produce leachates with high concentrations of metals (As, Cd, Cu, S y Zn).

f. According to the consulted literature, and composition and physicochemical properties found for these wastes, the SS could be an important secondary source of selenium, while both sludges could be used as a significant secondary source of lead. Se-Pb recovery can have remarkable economic and environmental benefits in contrast to their disposal in landfill.

g. The proposal for Se-Pb recovery consist in Se extraction from SS by using a roasting process, and then the calcined Pb-rich residue is blended with SC to recover Pb by hydrometallurgical route. The roasting process proposal could be an attractive option for Se recovery since roasting processes are widely used in primary copper refineries. On the other hand, Pb recovery by hydrometallurgy route would be the best option, considering that is one of the best alternative technology environmentally friendly.

h. In this sense, more researches are needed in order to evaluate the proposes alternative process to reuse these residues as a secondary source of Se and Pb.

Acknowledgements

This research was supported by the Atlantic Copper company project “Characterization of wastes from copper smelting and evaluation of potential applications”, and partially supported by the Spanish Government Department of Science and Technology (MINECO), through the project with reference: CTM2015-68628-R.

510 **References**

511 1. ICSG: The World Copper Factbook. (2018)

512 2. Newhook, R., Hirtle, H., Byrne, K., Meek, M.E.: Releases from copper smelters and refineries and
513 zinc plants in Canada: Human health exposure and risk characterization. Sci. Total Environ. 301,
514 23–41 (2003). https://doi.org/10.1016/S0048-9697(02)00229-2

515 3. Csavina, J., Taylor, M.P., Félix, O., Rine, K.P., Eduardo Sáez, A., Betterton, E.A.: Size-resolved
516 dust and aerosol contaminants associated with copper and lead smelting emissions: Implications
517 for emission management and human health. Sci. Total Environ. 493, 750–756 (2014).
518 https://doi.org/10.1016/j.scitotenv.2014.06.031

519 4. EEA: Circular by design: Products in the circular economy. (2017)

520 5. European Commision: Communication of 2.12.2015 on an EU action plan for the circular economy.
521 (2015). https://doi.org/10.1017/CBO9781107415324.004

522 6. Schlesinger, M.E., King, M.J., Sole, K.C., Davenport, W.G.: Extractive Metallurgy of Copper.
523 (2011)

524 7. Pérez, I., Moreno-Ventas, I., Ríos, G.: Chemical degradation of magnesia-chromite refractory used
525 in the conversion step of the pyrometallurgical copper-making process: A thermochemical
526 approach. Ceram. Int. 44, 18363–18375 (2018). https://doi.org/10.1016/j.ceramint.2018.07.052

527 8. Atlantic Copper: Annual Environmental Report. , Huelva (2017)

528 9. RD 1481/2001: Real Decreto 1481/2001 , de 27 de diciembre , por el que se regula la eliminación
529 de residuos mediante depósito en vertedero. (2013)

530 10. Directive 1999/31/EC: of the European Parliament and of the Council of 26 April 1999 on the
531 landfill of waste. (1999)

532 11. Yang, Z., Rui-Lin, M., Wang-Dong, N., Hui, W.: Selective leaching of base metals from copper
533 smelter slag. Hydrometallurgy. 103, 25–29 (2010). https://doi.org/10.1016/j.hydromet.2010.02.009

534 12. Lastra-Quintero, R., Rowlands, N., Rao, S.R., Finch, J.A.: Characterization and Separation of a
535 Copper Smelter Dust Residue. Can. Metall. Q. 26, 85–90 (2014).
536 https://doi.org/10.1179/cmq.1987.26.2.85

537 13. Nuñez, C., Espiell, F., Roca, A.: Recovery of copper, silver and zinc from Huelva (Spain) copper
538 smelter flue dust by a chloride leach process. Hydrometallurgy. 14, 93–103 (1985).
539 https://doi.org/10.1016/0304-386X(85)90008-8

540 14. Vircikova, E., Havlik, M.: Removing As from converter dust by a hydrometallurgical method. Jom.
541 51, 20–23 (1999). https://doi.org/10.1007/s11837-999-0152-1

542 15. Morales, A., Cruells, M., Roca, A., Bergó, R.: Treatment of copper flash smelter flue dusts for
543 copper and zinc extraction and arsenic stabilization. Hydrometallurgy. 105, 148–154 (2010).
544 https://doi.org/10.1016/j.hydromet.2010.09.001

545 16. Vítková, M., Ettler, V., Hyks, J., Astrup, T., Kříbek, B.: Leaching of metals from copper smelter
546 flue dust (Mufulira, Zambian Copperbelt). Appl. Geochemistry. 26, 263–266 (2011).
547 https://doi.org/10.1016/j.apgeochem.2011.03.120

548 17. González, A., Font, O., Moreno, N., Querol, X., Arancibia, N., Navia, R.: Copper Flash Smelting
549 Flue Dust as a Source of Germanium. Waste and Biomass Valorization. 8, 2121–2129 (2017).
550 https://doi.org/10.1007/s12649-016-9725-8

551 18. Font, O., Moreno, N., González, A., Querol, X., Navia, R.: Copper Smelting Flue Dust: A Potential
552 Source Of Germanium. Macla, Rev. la Soc. española Mineral. 15, 87–88 (2011)

553 19. Xing, P., Ma, B., Wang, C., Chen, Y.: Cleaning of lead smelting flue gas scrubber sludge and
554 recovery of lead, selenium and mercury by the hydrometallurgical route. Environ. Technol. (United
555 Kingdom). 39, 1461–1469 (2018). https://doi.org/10.1080/09593330.2017.1332102

556 20. Ha, T.K., Kwon, B.H., Park, K.S., Mohapatra, D.: Selective leaching and recovery of bismuth as
557 Bi2O3 from copper smelter converter dust. Sep. Purif. Technol. 142, 116–122 (2015).
558 https://doi.org/10.1016/j.seppur.2015.01.004

559 21. Balladares, E., Kelm, U., Helle, S., Parra, R., Araneda, E.: Chemical-mineralogical characterization
560 of copper smelting flue dust. Dyna. 81, 11 (2014). https://doi.org/10.15446/dyna.v81n186.32852

561 22. Pérez-Moreno, S.M., Gázquez, M.J., Ruiz-Oria, I., Ríos, G., Bolívar, J.P.: Diagnose for valorisation
562 of reprocessed slag cleaning furnace flue dust from copper smelting. J. Clean. Prod. 194, 383–395
563 (2018). https://doi.org/10.1016/j.jclepro.2018.05.090

564 23. Okanigbe, D.O., Popoola, A.P.I., Adeleke, A.A.: Characterization of Copper Smelter Dust for

565 Copper Recovery. Procedia Manuf. 7, 121–126 (2017).
566 https://doi.org/10.1016/j.promfg.2016.12.032

567 24. Mineralogy Database: Mineral Database,
568 http://webmineral.com/data/Anglesite.shtml#.XO_Hm4gzaUk

569 25. UNE-EN-12457-4: Caracterización de residuos. Lixiviación, Ensayo de conformidad para la
570 lixiviación de residuos granulares o lodos. (2003)

571 26. Al-Jabri, K.S., Al-Saidy, A.H., Taha, R.: Effect of copper slag as a fine aggregate on the properties
572 of cement mortars and concrete. Constr. Build. Mater. 25, 933–938 (2011).
573 https://doi.org/10.1016/j.conbuildmat.2010.06.090

574 27. Zhao, H., Xiao, Q., Huang, D., Zhang, S.: Influence of Pore Structure on Compressive Strength of
575 Cement Mortar. Sci. World J. 2014, 1–12 (2014). https://doi.org/10.1155/2014/247058

576 28. Murari, K., Siddique, R., Jain, K.K.: Use of waste copper slag, a sustainable material. J. Mater.
577 Cycles Waste Manag. 17, 13–26 (2014). https://doi.org/10.1007/s10163-014-0254-x

578 29. Wang, P.Z., Trettin, R., Rudert, V.: Effect of fineness and particle size distribution of granulated
579 blast-furnace slag on the hydraulic reactivity in cement systems. Adv. Cem. Res. 17, 161–166
580 (2005). https://doi.org/10.1680/adcr.2005.17.4.161

581 30. Khalid, M.K., Hamuyuni, J., Agarwal, V., Pihlasalo, J., Haapalainen, M., Lundström, M.: Sulfuric
582 acid leaching for capturing value from copper rich converter slag. J. Clean. Prod. 215, 1005–1013
583 (2019). https://doi.org/10.1016/j.jclepro.2019.01.083

584 31. Hansen, H.K., Yianatos, J.B., Ottosen, L.M.: Speciation and leachability of copper in mine tailings
585 from porphyry copper mining: Influence of particle size. Chemosphere. 60, 1497–1503 (2005).
586 https://doi.org/10.1016/j.chemosphere.2005.01.086

587 32. Montenegro, V., Sano, H., Fujisawa, T.: Recirculation of high arsenic content copper smelting dust
588 to smelting and converting processes. Miner. Eng. 49, 184–189 (2013).
589 https://doi.org/10.1016/J.MINENG.2010.03.020

590 33. Ramachandra Rao, S.: Chapter 10 Resource recovery from process wastes. In: Resource recovery
591 and recycling from metallurgical wastes. pp. 375–457 (2006)

592 34. Pérez-Moreno, S.M., Gázquez, M.J., Ruiz-Oria, I., Ríos, G., Bolívar, J.P.: Diagnose for valorisation

of reprocessed slag cleaning furnace flue dust from copper smelting. J. Clean. Prod. 194, 383–395 (2018). https://doi.org/10.1016/J.JCLEPRO.2018.05.090

35. Pérez, I., Moreno-Ventas, I., Parra, R., Ríos, G.: Post-mortem study of magnesia-chromiterefractory used in the gas area of a Submerged ArcFurnace for the copper-making process. Bol. la Soc. Esp. Ceram. y Vidr. 1–11 (2019). https://doi.org/10.1016/j.bsecv.2018.12.001

36. Olin, Å., Noläng, B., Osadchii, E.G., Öhman, L.-O., Rosén, E.: Chemical Thermodynamics of Selenium. (2010)

37. Hoffmann, J.E., King, M.J.: Selenium and Selenium Compounds. (2000)

38. Rumayor, M., Diaz-Somoano, M., Lopez-Anton, M.A., Martinez-Tarazona, M.R.: Mercury compounds characterization by thermal desorption. Talanta. 114, 318–322 (2013). https://doi.org/10.1016/j.talanta.2013.05.059

39. Kolta, G.A., Askar, M.H.: Thermal decomposition of some metal sulphates. Thermochim. Acta. 11, 65–72 (1975). https://doi.org/10.1016/0040-6031(75)80038-4

40. Ali, S., Sajadi, A.: A Comparative Investigation of Lead Sulfate and Lead Oxide Sulfate Study of Morphology and Thermal Decomposition. Am. J. Anal. Chem. 2, 206–211 (2011). https://doi.org/10.4236/ajac.2011.22024

41. Pérez-Moreno, S.M., Gázquez, M.J., Pérez-López, R., Bolivar, J.P.: Validation of the BCR sequential extraction procedure for natural radionuclides. Chemosphere. 198, 397–408 (2018). https://doi.org/10.1016/J.CHEMOSPHERE.2018.01.108

42. Król, A., Mizerna, K., Bożym, M.: An assessment of pH-dependent release and mobility of heavy metals from metallurgical slag. J. Hazard. Mater. 384, (2020). https://doi.org/10.1016/j.jhazmat.2019.121502

43. Caruso, B.S., Cox, T.J., Runkel, R.L., Velleux, M.L., Bencala, K.E., Nordstrom, D.K., Julien, P.Y., Butler, B.A., Alpers, C.N., Marion, A., Smith, K.S.: Metals fate and transport modelling in streams and watersheds: state of the science and USEPA workshop review B. Hydrol. Process. 22, 4011–4021 (2008). https://doi.org/10.1002/hyp

44. Hu, Z., Gao, S.: Upper crustal abundances of trace elements: A revision and update. Chem. Geol. 253, 205–221 (2008). https://doi.org/10.1016/j.chemgeo.2008.05.010

621 45. Földvári, M.: Handbook of Thermogravimetric System of Minerals and Its Use in Geological
622 Practice. (2011)

623 46. Mu, J., Perlmutter, D.D.: Thermal Decomposition of Inorganic Sulfates and Their Hydrates. Ind.
624 Eng. Chem. Process Des. Dev. 20, 640–646 (1981). https://doi.org/10.1021/i200015a010

625 47. Martínez Roca, J.: UNIVERSIDAD POLITÉCNICA DE CARTAGENA Escuela técnica superior
626 de Ingeniería Industrial. (2007)

627 48. Tagawa, H.: Thermal decomposition temperatures of metal sulfates. Thermochim. Acta. 80, 23–33
628 (1984). https://doi.org/10.1016/0040-6031(84)87181-6

629 49. Dunn, J.G., Muzenda, C.: Thermal oxidation of covellite (CuS). Thermochim. Acta. 369, 117–113
630 (2001)

631 50. Siriwardane, R. V., Poston, J.A., Fisher, E.P., Shen, M.S., Miltz, A.L.: Decomposition of the
632 sulfates of copper, iron (II), iron (III), nickel, and zinc: XPS, SEM, DRIFTS, XRD, and TGA study.
633 Appl. Surf. Sci. 152, 219–236 (1999). https://doi.org/10.1016/S0169-4332(99)00319-0

634 51. Chen, Y., Liao, T., Li, G., Chen, B., Shi, X.: Recovery of bismuth and arsenic from copper smelter
635 flue dusts after copper and zinc extraction. Miner. Eng. 39, 23–28 (2012).
636 https://doi.org/10.1016/j.mineng.2012.06.008

637 52. Wang, Q., Guo, X., Tian, Q., Jiang, T., Chen, M., Zhao, B.: Effects of matte grade on the
638 distribution of minor elements (Pb, Zn, As, Sb, and Bi) in the bottom blown copper smelting
639 process. Metals (Basel). 7, (2017). https://doi.org/10.3390/met7110502

640 53. Lucheva, B., ILiev, P., Kolev, D.: Hydro - pyrometallurgical treatment of copper converter flue
641 dust. J. Chem. Technol. Metall. 52, 320–325 (2017)

642 54. Wang, C., Li, S., Wang, H., Fu, J.: Selenium minerals and the recovery of selenium from copper
643 refinery anode slimes. J. South. African Inst. Min. Metall. 116, 593–600 (2016).
644 https://doi.org/10.17159/2411-9717/2016/v116n6a16

645 55. Kilic, Y., Kartal, G., Timur, S.: An investigation of copper and selenium recovery from copper
646 anode slimes. Int. J. Miner. Process. 124, 75–82 (2013).
647 https://doi.org/10.1016/j.minpro.2013.04.006

648 56. Hait, J., Jana, R.K., Sanyal, S.K.: Processing of copper electrorefining anode slime: a review.

649 Miner. Process. Extr. Metall. 118, 240–252 (2009). https://doi.org/10.1179/174328509x431463

650 57. Xiao, L., Wang, Y., Yu, Y., Fu, G., Liu, Y., Sun, Z., Ye, S.: Enhanced selective recovery of
651 selenium from anode slime using MnO 2 in dilute H 2 SO 4 solution as oxidant. J. Clean. Prod.
652 209, 494–504 (2019). https://doi.org/10.1016/j.jclepro.2018.10.144

653 58. Hoffmann, J.E.: Recovering selenium and tellurium from copper refinery slimes. Jom. 41, 33–38
654 (1989). https://doi.org/10.1007/BF03220269

655 59. Lin, X., Peng, Z., Yan, J., Li, Z., Hwang, J.Y., Zhang, Y., Li, G., Jiang, T.: Pyrometallurgical
656 recycling of electric arc furnace dust. J. Clean. Prod. 149, 1079–1100 (2017).
657 https://doi.org/10.1016/j.jclepro.2017.02.128

658 60. Mocellin, J., Mercier, G., Morel, J.L., Charbonnier, P., Blais, J.F., Simonnot, M.O.: Recovery of
659 zinc and manganese from pyrometallurgy sludge by hydrometallurgical processing. J. Clean. Prod.
660 168, 311–321 (2017). https://doi.org/10.1016/j.jclepro.2017.09.003

661 61. Ruşen, A., Sunkar, A.S., Topkaya, Y.A.: Zinc and lead extraction from Çinkur leach residues by
662 using hydrometallurgical method. Hydrometallurgy. 93, 45–50 (2008).
663 https://doi.org/10.1016/j.hydromet.2008.02.018

664 62. Shen, H., Forssberg, E.: An overview of recovery of metals from slags. Waste Manag. 23, 933–949
665 (2003). https://doi.org/10.1016/S0956-053X(02)00164-2

666 63. Öhrlund, I.: Future Metal Demand from Photovoltaic Cells and Wind Turbines - Investigating the
667 Potential Risk of Disabling a Shift to Renewable Energy Science and Technology Options Future
668 Metal Demand from Photovoltaic Cells and Wind Turbines Investigating the Potent. (2012)

669 64. The World Bank: The Growing Role of Minerals and Metals for a Low Carbon Future. (2017)

670 65. U.S. Geological Survey: Mineral Commodity Summaries 2019. (2019)

671 66. LME: London Metal Exchange: LME Lead, https://www.lme.com/Metals/Non-
672 ferrous/Lead#tabIndex=0

673 67. Svens, K.: Outokumpu Mercury Recovery. Met. News. 7, (1985)

674 68. Lee, W.R., Eom, Y., Lee, T.G.: Mercury recovery from mercury-containing wastes using a vacuum
675 thermal desorption system. Waste Manag. (2017). https://doi.org/10.1016/j.wasman.2016.12.017

69. Orhan, G.: Leaching and cementation of heavy metals from electric arc furnace dust in alkaline medium. Hydrometallurgy. 78, 236–245 (2005). https://doi.org/10.1016/J.HYDROMET.2005.03.002

70. Şahin, M., Erdem, M.: Cleaning of high lead-bearing zinc leaching residue by recovery of lead with alkaline leaching. Hydrometallurgy. 153, 170–178 (2015). https://doi.org/10.1016/J.HYDROMET.2015.03.003

71. BăDănoiu, G., Buzatu, T., Ghica, V.G., Buzatu, M., Iacob, G., Petrescu, I.M.: Study of PbSO4 solubilisation in NaOH solution, for the treatment of oxide-sulphate pastes obtained from dismembered lead-acid batteries. UPB Sci. Bull. Ser. B Chem. Mater. Sci. 76, 209–218 (2014)

72. Angelov, A., Groudev, S.: Treatment of gold-bearing solutions by cementation with metallic zinc. Min. Miner. Process. 44–45, 117–121 (2002)

73. Gouvea, L.R., Morais, C.A.: Recovery of zinc and cadmium from industrial waste by leaching/cementation. Miner. Eng. 20, 956–958 (2007). https://doi.org/10.1016/j.mineng.2007.04.016